High-speed modulation of a compact silicon ring resonator based on a reverse-biased pn diode

F.Y. Gardes[1]*, A. Brimont[2], P. Sanchis[2], G. Rasigade[3], D. Marris-Morini[3], L. O'Faolain[4], F. Dong[4], J.M. Fedeli[5], P. Dumon[6], L. Vivien[3], T.F. Krauss[4], G.T. Reed[1], J. Marti[2]

[1] *Advanced Technology Institute, University of Surrey*
Guildford, Surrey, GU2 7XH, UK
[2] *Nanophotonics Technology Center, Universidad Politécnica de Valencia,*
Camino de Vera s/n, 46022 Valencia, Spain
[3] *Institut d'Electronique Fondamentale, CNRS, Université Paris Sud*
91405 Orsay cedex, France
[4] *School of Physics & Astronomy, University of St Andrews*
North Haugh, St Andrews KY16 9SS, UK
[5] *CEA-Leti*
17 Rue des Martyr, 38054 Grenoble Cedex - France
[6] *Ghent University – IMEC*
Sint-Pietersnieuwstraat 4, 9000 Gent, Belgium
*F.gardes@surrey.ac.uk

Abstract: High speed modulation based on a compact silicon ring resonator operating in depletion mode is demonstrated. The device exhibits an electrical small signal bandwidth of 19GHz. The device is therefore a candidate for highly compact, wide bandwidth modulators for a variety of applications.

©2009 Optical Society of America

OCIS codes: (250.7360) Waveguide modulators; (230.2090) Electro-optical devices; (250.5300) Photonic integrated circuits; (230.5750) Resonators

References and links

1. R. A. Soref, and B. R. Benett, "Electrooptical effects in Silicon," IEEE J. Quantum Electron. **23**(1), 123–129 (1987).
2. F. Y. Gardes, G. T. Reed, N. G. Emerson, and C. E. Png, "A sub-micron depletion-type photonic modulator in silicon on insulator," Opt. Express **13**(22), 8845–8854 (2005).
3. D. Marris, E. Cassan, and L. Vivien, "Response time analysis of SiGe/Si modulation-doped multiple-quantum-well structures for optical modulation," J. Appl. Phys. **96**(11), 6109–6111 (2004).
4. A. Liu, L. Liao, D. Rubin, H. Nguyen, B. Ciftcioglu, Y. Chetrit, N. Izhaky, and M. Paniccia, "High-speed optical modulation based on carrier depletion in a silicon waveguide," Opt. Express **15**(2), 660–668 (2007).
5. D. Marris-Morini, L. Vivien, J. M. Fédéli, E. Cassan, P. Lyan, and S. Laval, "Low loss and high speed silicon optical modulator based on a lateral carrier depletion structure," Opt. Express **16**(1), 334–339 (2008).
6. A. Liu, L. Liao, D. Rubin, J. Basak, Y. Chetrit, H. Nguyen, R. Cohen, N. Izhaky and M. Paniccia, "Recent development in a high-speed silicon optical modulator based on reverse-biased pn diode in a silicon waveguide," Semicond. Sci. Technol. **23**(064001), 1–7 (2008).
7. C. Gunn, "CMOS Photonics for High-Speed Interconnects," Micro, IEEE **26**(2), 58–66 (2006).
8. Q. Xu, S. Manipatruni, B. Schmidt, J. Shakya, and M. Lipson, "12.5 Gbit/s carrier-injection-based silicon micro-ring silicon modulators," Opt. Express **15**(2), 430–436 (2007).
9. J. B. You, M. Park, J. W. Park, and G. Kim, "12.5 Gbps optical modulation of silicon racetrack resonator based on carrier-depletion in asymmetric p-n diode," Opt. Express **16**(22), 18340–18344 (2008).
10. Surrey Ion Beam Centre implantation facility, *http://www.ionbeamcentre.co.uk/*, CEA Leti, *http://www-leti.cea.fr*
11. T. Alzanki, R. Gwilliam, N. Emerson, and B. J. Sealy, "Differential Hall effect profiling of ultrashallow junctions in Sb implanted silicon," Appl. Phys. Lett. **85**(11), 1979–1980 (2004).

1. Introduction

High speed modulators are a key building block for a variety of integrated photonic functions, such as optical interconnects, on-chip clock and data distribution and optical signal processing. Among the different technologies proposed to develop modulators, silicon photonics is one of the most promising as it allows mass production at competitive cost and

the development of complex optical functionalities monolithically integrated with advanced electronics in single all silicon chips. The plasma dispersion effect has been demonstrated as the most effective way to modulate the refraction index in silicon [1]. Demonstrations of high speed (multi- GHz) modulation in free carrier depleted silicon-based modulators have been made theoretically [2,3] and experimentally [4–7]. However, the need for compactness, the key for VLSI (Very Large Scale Integration), has motivated the development of small resonant structures among other alternatives. The use of a ring resonator via carrier injection, to modulate an optical signal has already been shown in [8] to reach bit rates as high as 12.5 Gbit/s under a pre-emphasized voltage driving scheme. Recently, high speed optical modulation using carrier depletion in an asymmetric silicon p-n diode resonator has been demonstrated [9]. However, the device showed only a 3 dB bandwidth of 8 GHz and data transmission up to 12.5 Gbit/s. Furthermore, the pn junction was formed in a wide silicon waveguide (600 nm x 600 nm). In this paper, a high-speed silicon modulator based on carrier depletion in a reverse-biased pn junction is demonstrated. In this case, the pn junction is formed in a compact and standard silicon waveguide with 300 nm width and 200 nm height. This results in a very compact modulator with a footprint lower than 100 μm^2.

2. Design and fabrication

The proposed ring resonator modulator is based on a 300 nm wide, 150 nm etch depth and 200 nm high rib waveguide, which enables single mode transmission. As shown in Fig. 1, the pn junction is asymmetrical in size and in doping concentration in order to maximize the area of hole depletion that overlaps with the optical mode. The n-type region is 75 nm wide and the p type 225 nm wide, and the net doping concentration of this particular junction varies between 6x 10^{17} /cm3 and 2x10^{17} /cm3, for n and p types, respectively. The junction is fabricated using ion implantation at Leti and the IBC [10]. Boron is first implanted and annealed to form a uniform p type background doping, then a series of antimony implants at different energies in the centre of the ring are used to form the n type area of the pn junction. Antimony was specifically selected for its low straggle and low diffusion characteristics to avoid redistribution of the n type doping in the waveguide. The resistive contacts are formed by highly doped regions (1x10^{20} /cm3) of boron and phosphorus and are placed 1µm away from the junction to minimise interaction with the optical mode and thus absorption losses. A final anneal was performed by rapid thermal annealing at 1050 °C for 10 seconds to activate the doping regions. The position of the contact electrodes, as well as the highly doped regions, are key to the performance of a reverse biased pn based-modulator because the frequency response is limited by the RC cut off frequency resulting from capacitive effects within the junction and the resistance of the doped regions and metal contacts.
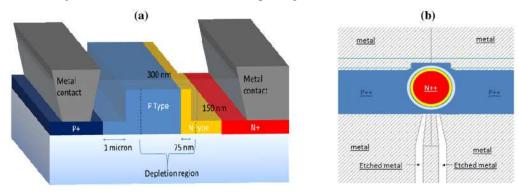

Fig. 1. (a) Cross section and (b) top view of the device.

The optical structures were fabricated using 193 nm deep UV (DUV) lithography whilst doping regions were fabricated by means of ion beam implantation. The resist windows for the p and n doping steps were defined using DUV lithography, while those for the p++ and n++

were defined using Electron Beam Lithography (EBL). After doping, the sample was covered with a layer of spin-on glass (Dow Corning Fox-14) and hardbaked, providing electrical insulation and minimising the interaction of the optical mode with the metal .Windows were opened in the oxide above the p^{++} and n^{++} contacts (defined using EBL). Titanium/Aluminium contacts were then deposited using a liftoff technique and annealed at 450 °C to form the electrode inside and around the ring shown Fig. 2 (a) and Fig. 2 (b).

Fig. 2. Scanning Electron Microscope (SEM) image of ring resonator based modulator with a 5 microns ring radius (a) before and (b) for different radius size after contacts deposition.

3. Experimental results

The experimental set-up uses a tunable laser from 1520 to 1620 nm. A linearly TE polarized light beam is coupled into the waveguide using a polarization-maintaining lensed-fiber. The output light is collected by an objective and focused on an IR detector. The output spectrum of the modulator with no bias is reported in Fig. 3 (a). The free-spectral range of the 40.2 microns circumference ring resonator varies from 2.5 nm at 1520 nm to 3 nm at 1620 nm. The spectrum shows resonant drops larger than 20 dB around 1580 nm where the quality factor is Q = 3130.

Electrical probes were used to bias the diode. Very low values of the reverse current (−1 µA at −10 V) were measured that ensured low electrical power dissipation in the ring resonator. With reverse voltage bias, carrier depletion is responsible for refractive index change in the waveguide, which results in a red shift of the spectrum.
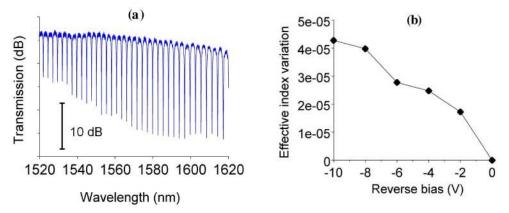

Fig. 3. (a) Experimental ring resonator transmission with no bias. (b) Experimental effective index variation as a function of reverse bias.

A shift in resonant wavelength was measured at −10 V giving rise to a DC on/off ratio of 5 dB. The effective index variation of the guided mode in the ring resonator was deduced from wavelength shifts using the following relation:

$$\Delta n_{eff} = \frac{\Delta \lambda}{\lambda} n_g \qquad (1)$$

where the group index n_g is deduced from the free-spectral range measurement. The effective index variation as a function of the reverse biased is reported in Fig. 3 (b). An effective index variation of 4.10^{-5} is measured at −10 V.

The frequency response of the modulator was measured using an AC signal generated by an opto-RF vector network analyser (Agilent 86030A). The RF signal was coupled to the ring resonator using ground-signal-ground electrodes. The modulated optical signal was then coupled back to the opto-RF vector network analyser. The normalized optical response as a function of the frequency is given in Fig. 4. A 3 dB cut-off frequency of 19 GHz is measured.
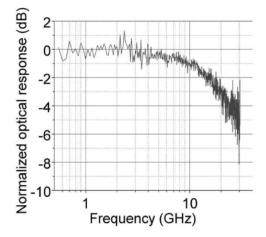

Fig. 4. Normalized optical response as a function of frequency.

The fabricated device displays promising figures in terms of frequency of operation, however the change in effective refractive index achieved is less than that expected. We believe that this is due to problems with the alignment and dopant activations for which we try to give an explanation in the paragraph below. These problems can be overcome in the next generation of devices by moving towards a process with a self aligned junction and a different impurity selection for the waveguide n type doping. This would enable a greater process control and increase the device yield.

4. Analysis of results

The modulator performance was simulated using Athena for the process development and ion implantations, and Atlas for DC and transient analysis, both part of the semiconductor CAD software Silvaco. Optical characteristics for the efficiency and transient analysis were calculated using an in house mode solver. A maximum efficiency of $V_\pi \cdot L_\pi$ =3.46 V.cm was obtained at the optimum position of the junction. However, the simulations show that the alignment of the n type implant is indeed critical. Figure 5 shows the simulated change in effective index against the position of the junction in the waveguide for increasing reverse bias for which the implantation doses and energies used during fabrication stay the same. It is clear by analysing the data that as the junction moves away from the optimum position, the efficiency of the device decreases. To give an example, when the alignment error of the n type area is 150 nm towards the centre of the waveguide then the VπLπ will be decreased to 9.1 V.cm.
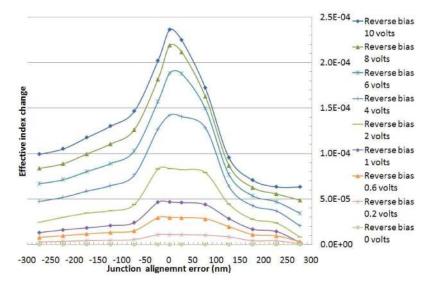
Fig. 5. Junction alignment error in nm against effective index change for increasing reverse voltages in volts.

On the other hand, the fabricated device was produced using three different impurities, phosphorus, boron and antimony. If one of the doping species implanted into the waveguide is not fully activated during rapid thermal annealing, the efficiency will also decrease. In this device, activation of antimony could be an issue, as studies from Alzanki et al [11] showed that anneal temperatures above 950 °C could lead to a decrease in activation. Figure 6 shows the effect of decreasing the antimony activation on the effective index change for a reverse bias of −10 volts and for different positions of the junction. It is clear that the activation of antimony also has a significant impact on the efficiency of the device.
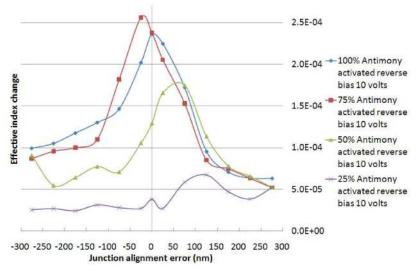

Fig. 6. Junction alignment error against effective index change for a 10 volt reverse voltage with decreasing antimony activation.

The effect is such that the device efficiency is decreased from 3.46 V.cm for a 100% antimony activation to below 12 V.cm when the antimony activation is around 25%. The measured effective index change of 4.10^{-5} for a reverse bias of −10 Volts, is consistent with the simulated efficiency for an activation of 25% of the antimony. This correlates well with

the results of Alzanki et al [11] who measured a decrease of the activation of antimony to 25% when the anneal temperature reached 1050°C for 10 seconds, as was used during the processing of this specific device. Simulations were performed with the actual thickness of the fabricated device which was measured to be 67 nm instead of 50 nm and showed the intrinsic bandwidth to be around 30 GHz for 100% Antimony activation and to be more than 50 GHz for 25% Antimony activation. The decrease of the capacitance due to deactivation of Antimony explain the increase of the intrinsic operating bandwidth. The bandwidth value measured at 19 GHz leaves room for further improvements on the electrode design and resistive contact positioning to enable even better performances.

5. Conclusions

In conclusion, we present a high speed ring resonator modulator based on the carrier depletion effect in an asymmetric pn diode structure. The modulator exhibited a DC on/off ratio of 5 dB at −10 V, and a 3 dB bandwidth of 19 GHz. Furthermore, despite the relatively high bandwidth result, the device is non-optimal, which can be attributed to misalignment of the junction and incomplete activation of the dopants used to form the pn junction. Consequently, the next generation of devices is expected to perform significantly better.

Acknowledgments